Heliyon 10 (2024) e36303

Contents lists available at ScienceDirect

Heliyon

journal homepage: www.cell.com/heliyon

Research article

Identification of response regulation governing ozone formation based on influential factors using a random forest approach

Yan Huang [a,b], Qingqing Wang [a], Xiaojie Ou [b], Dongping Sheng [b], Shengdong Yao [b], Chengzhi Wu [c,**], Qiaoli Wang [b,*]

[a] Ecological Environmental Monitoring Station of Deqing County, Huzhou, 313200, China
[b] College of Environment, Zhejiang University of Technology, Hangzhou, 310032, China
[c] Trinity Consultants, Inc. (China Office), Hangzhou, 310012, China

ARTICLE INFO

Keywords:
Ozone
Response regulation
Influence factors
Random forest
Sensitive analysis

ABSTRACT

The pursuit of enhanced scientific, refined, and precise ozone and air quality control continues to pose significant challenges. Using data visualization techniques and random forest (RF) algorithms, the temporal distribution of atmospheric pollutants and the interrelationship between O_3 concentration and its influential factors were investigated with one-year monitoring data in Deqing county in 2021. The local atmospheric conditions predominantly belonged to NOx-sensitive and transition zone. Extremely high O_3 concentration were primarily observed when temperatures (T) exceeded 30 °C, with relative humidity (RH) ranging between 30 and 60 %. NO_2, RH and T were identified as the top 3 important factors, and O_3 concentration have stronger linearly relationship to RH and T, while stronger nonlinearly relationship to NO_2. By employing an optimized RF model, controlling consistent mild and high reaction atmospheric conditions, the O_3 concentration response to the change of individual influencing factors was acquired. The O_3 concentration increased and then decreased in response to the increasing NO_2 concentration, displaying a characteristic inflection point at 10 μg m^{-3}. More reactive radicals produced at higher VOCs concentration and continuing NO*x* cycle at lower NO_2 concentration, resulting in the acceleration in the direction of producing more O_3. Therefore, the significant different O_3 response to variation of VOCs and NO*x* concentration between mild and high reaction atmospheric conditions, as well as the existing of oxidant elevation should be considered in local air quality control. This study demonstrates the efficacy of ML methods in simulating nonlinear response of O_3, supports the understanding of local O_3 formation and quick guidance for precise local O_3 pollution control and the related strategies.

1. Introduction

Air pollution stands as a pivotal concern deeply impacting our daily lives [1–3]. Remarkable strides have been made in enhancing air quality in China, evidenced by the significantly decrease in particles concentration [1,4–6] due to a series of policies and actions, notably the campaign of Winning the Blue Sky War and the action plan of Air Pollution Prevention and Control. However, the severity

* Corresponding author.
** Corresponding author.
E-mail addresses: CWu@trinityconsultants.com (C. Wu), wangqiaoli@zjut.edu.cn (Q. Wang).

https://doi.org/10.1016/j.heliyon.2024.e36303
Received 23 January 2024; Received in revised form 4 August 2024; Accepted 13 August 2024
Available online 14 August 2024

of ozone pollution has been increasing, surpassing $PM_{2.5}$ as the predominant pollutant, particularly during the summer and autumn seasons. The understanding of O_3 formation regulations remains inadequate due to the variations in atmospheric conditions and the emission of O_3 precursors are different across regions [3,7]. The pursuit of achieving more scientific, refined, precise ozone and air quality control continues to present significant challenges.

The implementation of Ambient air quality standards (GB 3095–2012) in China has led to the continuous refinement of the monitoring network, including 6 general pollutants of SO_2, NO_2, CO, $PM_{2.5}$, PM_{10} and O_3, as well as meteorological elements containing temperature (T), pressure (P), relative humidity (RH), wind direction (WD) and wind speed (WS) [8–10]. A significant disparity was observed in the spatiotemporal distribution of air pollutants based on long-term monitoring data from national monitoring stations [11,12]. The mounting evidence has unequivocally demonstrated that the formation of O_3 is governed by the concentrations of VOCs and NO*x* [13–15], while the O_3 response to the changes in those precursors is complex, and formulating universal regulations proves challenging [16,17]. Meanwhile, an increasing number of monitoring sites have implemented VOC detection equipment to measure the concentration of various VOC species [18,19], which help understanding the response of O_3 formation from the intricate temporal variation regulations between O_3 and its precursors [20]. Based on 1-year continuous observations, a comprehensive analysis was conducted to examine the diurnal and seasonal characteristics of regional O_3 concentration, as well as the potential for O_3 generation associated with different VOC species [21]. Additionally, certain research efforts were dedicated to identifying influential factors and investigating specific episodes of elevated ozone levels [22,23].

Chemical transport models (CTMs), incorporating the latest advancements in atmospheric science, serve as widely utilized tools to simulate the complex chemical and physical processes involved in ozone formation in large-scale areas. While the EKMA (Empirical Kinetic Modeling Approach) curve generated by box models, including the MCM (Master Chemical Mechanism) or OZIPR (Ozone Isopleth Plotting Program) models, is extensively employed to depict the in-situ correlation between ozone, NOx, and VOCs concentrations in local regions [15]. These models offer practicality in assessing the relative contributions and sensitivity of emission sources; however, their inability in predicting the responses to the changes in emission oriented from policy-relevant scenarios limit their applicability, as well as their computational complexity [24].

With the advancement of data science and machine learning (ML) techniques, there has been a growing emphasis on their application in air quality assessment and prediction of ozone formation [25], which have even been observed satisfactory prediction performance in both individually application and supporting to enhance the simulation of CTMs [24]. For example, regression algorithms [26], random forest (RF) [27], artificial neural network (ANN) [20,28], convolutional neural network (CNN) [29], as well as hybrid deep learning modes [30–32] have different applications and expressed great visualization ability and high simulation performance, verifying the validation of ML techniques in prediction ozone formation. In current reported studies, ML techniques are

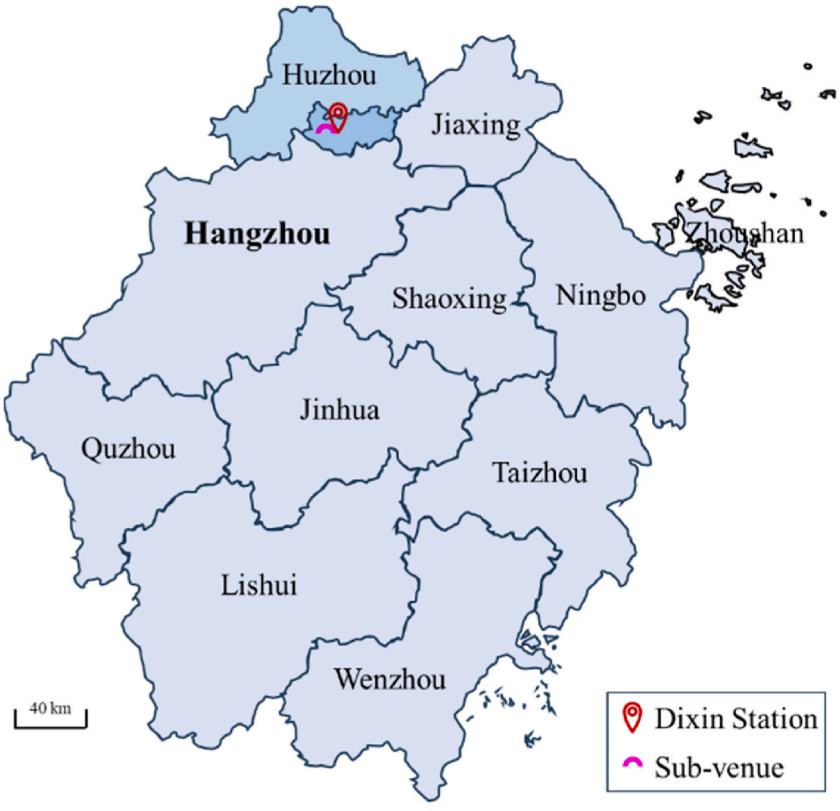

Fig. 1. The study area is situated in Deqing, Zhejiang Province.

mostly applied to improve the simulation performance of air quality models, to enhance the forecast accuracy of ozone concentrations in the upcoming days, to discover the emission characteristics of VOCs source profiles. However, the majority of these optimized models have primarily been employed for future O_3 concentration prediction, although some studies on ozone formation regulation were carried out applying multiple linear regression method, with limited application in elucidating the interrelationship of formation response in O_3 concentrations with the changes in VOCs and NOx concentrations [20]. RF is an ensemble supervised learning method, in comparisons with other modeling method, RF models demonstrated superiorities in minimizing error [33–35]. Besides, the importance evaluation of RF provides some explanation on the contribution of variables to ozone formation.

Therefore, this study conducted a comprehensive 1-year analysis applying the monitoring data from a standard continuous air quality monitoring station in Deqing county. Applying different data analysis approaches and RF simulation, statistical analysis was conducted to determine the key variables and their impact on O_3 formation, considering the influence of other pollutants and meteorological factors. The findings demonstrate the efficacy of ML approaches in capturing the nonlinearity response of ozone to influential pollutants and meteorological factors, highlighting the potential of this novel method to complement and enhance our understanding of local O_3 formation mechanisms in complex environments. Moreover, it provides a scientific and effective framework for guiding rapid, comprehensive, and precise air pollution control strategies during significant events.

2. Materials and methods

2.1. Study area

The study selects Deqing county, which serves as the permanent site for the United Nations Geographic Information Congress and a sub-venue for volleyball during the 2022 Hangzhou Asian Games, as depicted in Fig. 1. Located within Huzhou city and situated in the heartland of the Yangtze River Delta, Deqing county experiences a north subtropical monsoon climate characterized by four distinct seasons, abundant rainfall, ample sunlight, and warm humidity. The average annual temperature ranges from approximately 13-16 °C with January being the coldest month and July being the hottest.

Deqing county takes pride in its robust industrial sector, which encompasses diverse fields such as biotechnology and pharmaceuticals, manufacturing enterprises, innovative building materials, as well as machinery industries. Moreover, it owns robust transportation infrastructure as a tourist city and the possession of the Deqing Port International Logistics Park, which further enhances its connectivity. Conversely, it also faces significant air pollution resulting from industrial and transportation emissions, particularly high O_3 pollution, ranged from 150 to 171 μg m^{-3} in 2019–2022 with the annual average concentration.

2.2. Data source

In order to predict O_3 concentration through general Monitoring factors, as only basic meteorological parameters are hourly monitored in most local monitoring stations [36], air pollutants factors of SO_2, NO_2, CO, $PM_{2.5}$, PM_{10}, O_3, VOCs, and meteorological elements of T, P, RH, WD, WS in 2021 were extracted from the Dixin site in Deqing county. The monitoring data was measured following the technical specifications of *Automated methods for ambient air quality monitoring* (HJ/T 193), *Technical specifications for operation and quality control of ambient air quality continuous automated monitoring system for SO_2, NO_2, O_3 and CO* (HJ 818), *Specifications and Test Procedures for Ambient Air Quality Continuous Monitoring System with Gas Chromatography for Volatile Organic Compounds* (HJ 1010) and *Specifications and test procedures for ambient air quality continuous automated monitoring system for PM_{10} and $PM_{2.5}$* (HJ 653) [37,38]. Though $PM_{2.5}$, PM_{10}, and SO_2 are not O_3 precursors and not strongly related to O_3, they are included in the ML model to enhance the prediction performance [24,39]. The temporal distribution of those factors was shown in Fig. S1. Totally, 8760 samples were acquired setting each monitoring hour as an individual sample, with some missing data recorded as null, due to devices maintenance. Meanwhile, the hourly observation data of general air pollutants and meteorological elements were also expressed in Fig. S2.

2.3. Random forest (RF)

RF is an ensemble learning method that operates by constructing a multitude of decision trees [33]. In this study, a RF model was developed with the influencing factors as input and the O_3 concentrations as output as the followed equation (3):

$$Y_i(O_3) = f(Time_i, c_i(VOCs), c_i(SO_2), c_i(NO_2), c_i(CO), c_i(PM_{2.5}), c_i(PM_{10}), T_i, P_i, RH_i, WD_i, WS_i) \quad (3)$$

Where, $Y_i(O_3)$ referred to the ith output of O_3 concentrations in simulation; i referred to each observation sample; c_i referred to the ith concentrations of each influencing pollutants.

The sample set was pre-divided into a simulation set and a validation set by extracting 1 sample out of every 15 samples, ensuring coverage across the entire observation period. Only the simulation set was utilized for RF training, which was further divided into a training set and a test set based on a 5-fold cross-validation. The trees were set 100 firstly, and the best leaves were searched by setting leaf number from 3 to 10. The simulation results showed convergent earlier than 100 trees, considering good stability, the number of trees was finally set 100. As to the number of leaves, the errors of each leaf setting was extracted and the best leaves was 7. Hence, the

final parameters of trees and leaves were set 100 and 7 after optimization, when R^2 and Error were applied to evaluate the simulation performance. After optimization, 200 times repeat simulation was executed with the optimized trees and leaves to minimize the impact of randomness.

Additionally, in RF, feature importance analysis has been proven as an effective approach to quantitatively assess the predictive capability of input features on model outputs [40]. The importance of each variable was extracted from the optimized RF model for further analysis.

3. Results and discussions

3.1. Temporal distribution

Hourly observation data and daily average values were monthly statistically analyzed, as shown in Fig. 2. The VOCs concentration mainly distributed within 10^2–10^3, of 420.25 μg m^{-3} annually averagely, with a happened high value of 142299.83 μg m^{-3}, as shown in Fig. 2(a). VOCs pollution conditions mostly occurred in Apr. and Nov., due to the moderate temperatures for facilitate volatilization and atmospheric oxidation. Relatively higher concentrations were observed for SO_2, NO_2, CO, $PM_{2.5}$ and PM_{10} in winter, as shown in

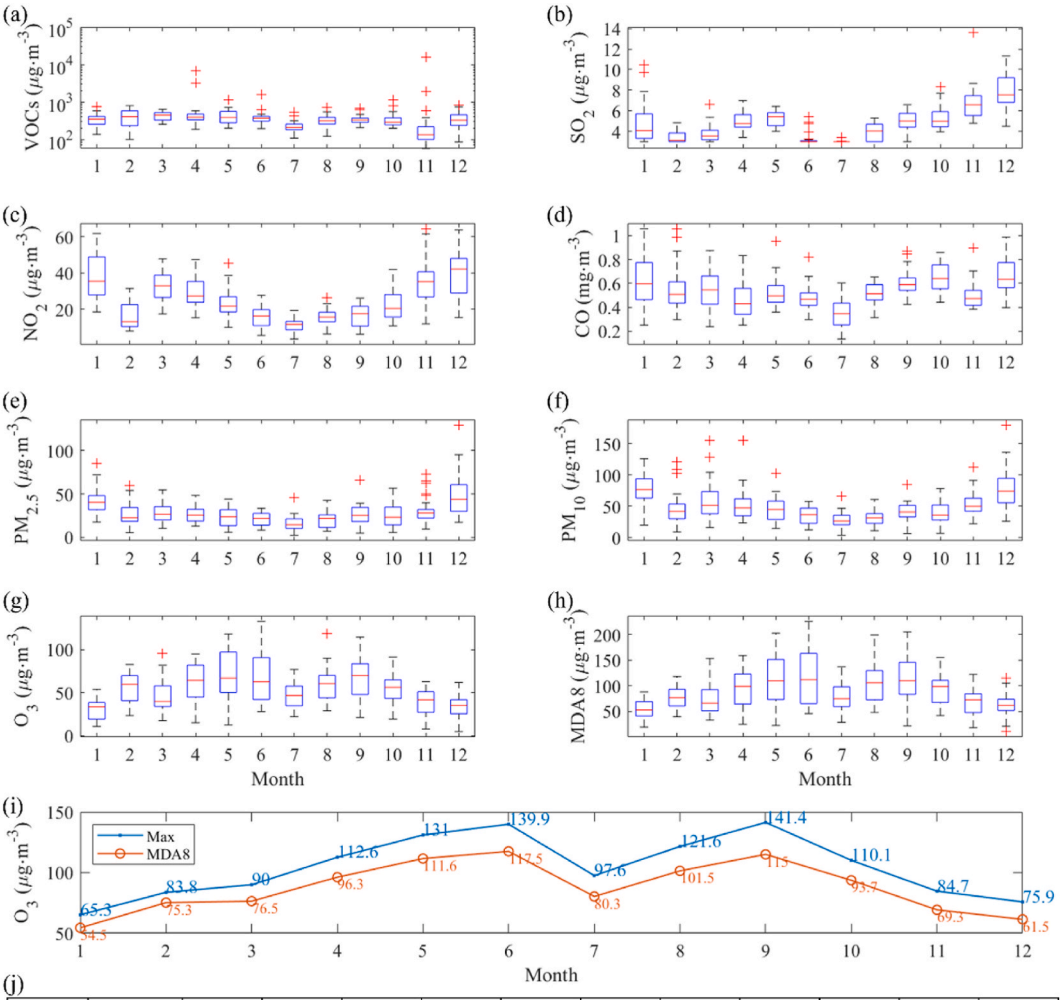

(j)

Pollutant	VOCs	SO_2	NO_2	CO	$PM_{2.5}$	PM_{10}	O_3	T	P	RH	WD	WS
Unit	μg/m^{-3}	μg/m^{-3}	μg/m^{-3}	mg/m^{-3}	μg/m^{-3}	μg/m^{-3}	μg/m^{-3}	℃	hPa	%	°	m/s
Mean	420.25	4.8	24.7	0.54	28.0	48.7	53.2	18.8	1014.74	75.1	155.6	1.37
Max	142299.83	36.0	120.0	1.60	193.0	443.0	286.0	38.1	1042.10	100.0	317.7	7.75
Min	1.58	3.0	2.0	0.10	2.0	3.0	2.0	-5.8	986.36	17.1	0.0	0.07

Fig. 2. Monthly distribution air pollutants and meteorological elements in each month. (a) VOCs, (b) SO_2, (c) NO_2, (d) CO, (e) $PM_{2.5}$, (f) PM_{10}, (g) O_3, (h) MDA8, (i) Maximum and MDA8 concentration of O_3 and (j) Statistical values.

Fig. 2(b)–(f), besides the low NO_2 concentration in Feb. because of the lower traffic during Spring Festival, as shown in Fig. S2. The daily average concentrations of SO_2, NO_2 and CO have met the national air quality standard, while still some hours exceeding the daily $PM_{2.5}$ and PM_{10} standards of 75 μg m^{-3} and 150 μg m^{-3}. As shown in Fig. 2(g)–(i), the O_3 pollution was commonly expressed by the maximum daily 8-h average concentration (MDA8) of 160 μg m^{-3} as the national standard. High MDA8 concentration mostly occurred in Jun. and Sep., with the highest MDA8 value reached 225.9 μg m^{-3} in 2021. Therefore, O_3 should be given primary consideration in local air quality control. In terms of meteorological elements, typically subtropical monsoon climate was observed, with the highest temperature of 38.1 °C in Jul., stable wind speed of mostly slower than 2 m s^{-1}, as shown in Fig. 2(j).

The average concentration of pollutants was computed on an hourly basis for further analysis in Fig. S3. The distribution of CO, SO_2, $PM_{2.5}$ and PM_{10} were relatively stable within each day. While that of NO_2 exhibited a slight trough at 2 p.m., attributed to reduced vehicular emissions during non-peak hours and enhanced elimination due to intensified solar radiation [21,41]. Additionally, the distribution of VOCs expressed two peaks of an extremely high peak at 11 a.m. and another at 5 p.m. partially resulting from sufficient plant activity and industrial emission. Similar with other typical distributions [15,21], the O_3 concentration reached its maximum, which peaked at 15:00 and recorded at 93 μg m^{-3} averagely in Dixin site in 2021, due to photochemical reactions, and subsequently declined.

3.2. Simulation and importance identification

The formation of O_3 can be influenced by numerous factors, such as coexisting ambient pollutants and meteorological elements. RF model was trained to predict the concentration of O_3, which is driven by observation data of its influencing factors. The model was optimized by parameters of trees and leaves. Due to the refined monitoring data and the strong adaptability of RF algorithm, comparing to other studies [26,42], the built model demonstrated exceptional performance and generalization ability, as shown in Fig. S4, with R^2 values of 0.975, 0.945, and 0.946 for the training set, test set, and verification set respectively.

Based on the optimized parameters, 200 times of RF training were conducted, and the importance evaluation of each training was extracted, as shown in Fig. 3. The distribution of importance evaluation exhibited a relatively consistent pattern. By sorting the average importance of the 200 times training, NO_2, RH and T were identified as the top 3 important factors, while interestingly, the importance of VOCs on O_3 prediction was weak. In comparison with other studies, notably high contributions of RH and T were observed in the Yangtze River Delta and North China Plain regions in China, respectively [43].

3.3. O_3 formation sensitive factors

In order to ascertain the importance on predicting O_3 concentration, the *Pearson* correlations among the monitored factors were computed, as depicted in Fig. 4(a). Similar to the importance evaluation, the top 3 highest correlations with O_3 concentration observed for NO_2, RH and T; however, they exhibited different sort of −0.55, 0.44 and −0.42 for RH, T and NO_2. Similar important factors were also observed in other areas [20,44].

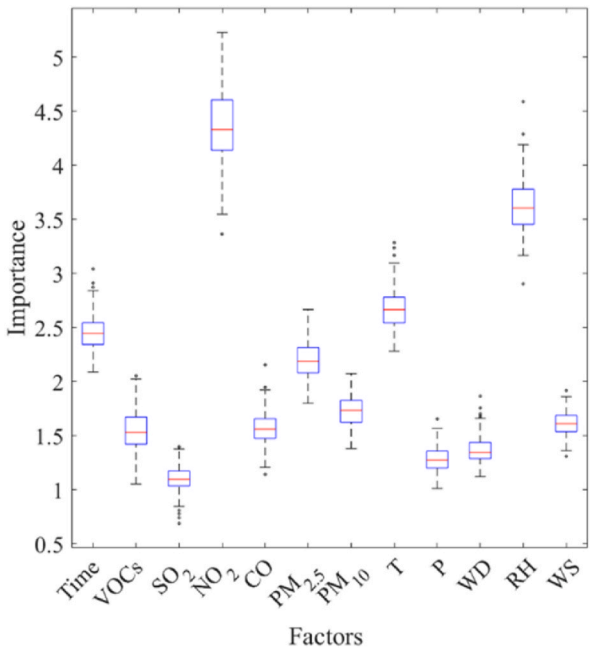

Fig. 3. Importance identification distribution of 200 times of RF training.

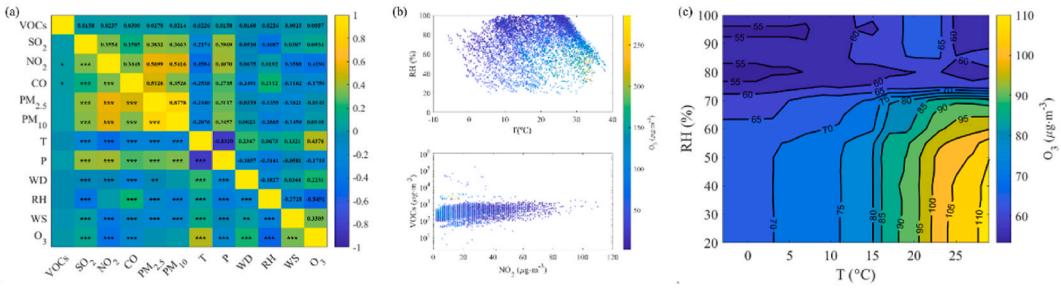

Fig. 4. Distribution of O_3 to sensitive factors by (a) *Pearson* correlation, (b) Scatter distribution and (c) Contour distribution.

Less correlation was revealed in VOCs to both other factors and O_3 concentration. The lack of correlation of VOCs can be attributed to the diverse of VOCs sources, the variational concentration distribution of VOC species and the discrepant chemical reactivity of individual VOC species. Incidentally, SO_2 revealed a negative correlation of −0.41 to RH, due to its characteristic of solubility and reactivity with H_2O. NO_2 had positive correlations to $PM_{2.5}$ and PM_{10}, since NO_2 also acts as one of the precursors of secondary particles.

Additionally, the scatter distribution of O_3 to the top 3 factors and VOCs were further analyzed, as shown in Fig. 4(b). The occurrence of high O3 pollution is predominantly associated with meteorological conditions characterized by elevated temperatures above 15 °C and RH ranging from 20 % to 70 %. Furthermore, extremely high O_3 are primarily observed under more stringent conditions, with high temperatures exceeding 30 °C and RH levels ranging from 30 % to 60 %.

The correlation between O_3 and VOCs was found to be negligible, whereas a strong correlation was observed between O_3 and NO_2, indicating that the concentration of O_3 is more sensitive to changes in atmospheric NO_2 concentration than VOCs. As the concentration of NO_2 decreases, the O_3 concentration is more likely to increase. Furthermore, high concentrations of O_3 were predominantly observed when the NO_2 under a concentration within 10 μg m^{-3} and 30 μg m^{-3}. Besides, the O_3 concentration effected by T and RH was further investigated by setting other variables at average values in RF model. As shown in Fig. 4(c), the O_3 concentration revealed obviously changes to RH and T. The concentration of O_3 increased with the increase of T. Meanwhile, when RH is lower than about 40 %, the change in O_3 concentrations shows limited. The O_3 concentration decreases with the increase in RH, at moderate RH between 40 % and 70 %. Interestingly, the O_3 concentration remains relatively low and appears to be less influenced by RH and T when the RH exceeds 70 %.

The dominant influence of VOCs and NO_2 on O_3 formation among ambient pollutants has been consistently demonstrated in numerous studies [45–47], but the results in Figs. 3 and 4 showed that VOCs expressed less importance and correlation to O_3. According to the basic photochemical reactions, the change in O_3 concentration is not only controlled by the absolute concentrations, but also the relative reactivity of the precursors [48]. Different ratios can be indicator to infer the sensitive of O_3 concentration on precursors, such as NOy, HCHO/NOy, HCHO/NO_2, VOCs/NO_2 [49–51]. When the VOCs/NO_2 ratio is low, the reaction between OH radical and NO_2 is predominant, while O_3 generation is highly influenced by VOCs that belongs to VOCs-sensitive region. Conversely, O_3 is more sensitive to NO_2 as the NO_2-sensitive region, with the O_3 contour ridge of 5–11 for volume fraction [41,52,53], or about 8–22 for mass fraction [54]. However, the judgement of the transition from different sensitive zones varies across regions because of the different background atmospheric conditions [47,55]. Overall, the sensitivity is determined by the extent of changes in O_3 concentration induced by the precursors. Thus, considering the significant affection of the ratio of VOCs and NO_2 on O_3 concentrations, this ratio was calculated and visualized in probability density figure, as shown in Fig. 5(a). The ratio of VOCs/NO_2 is predominantly

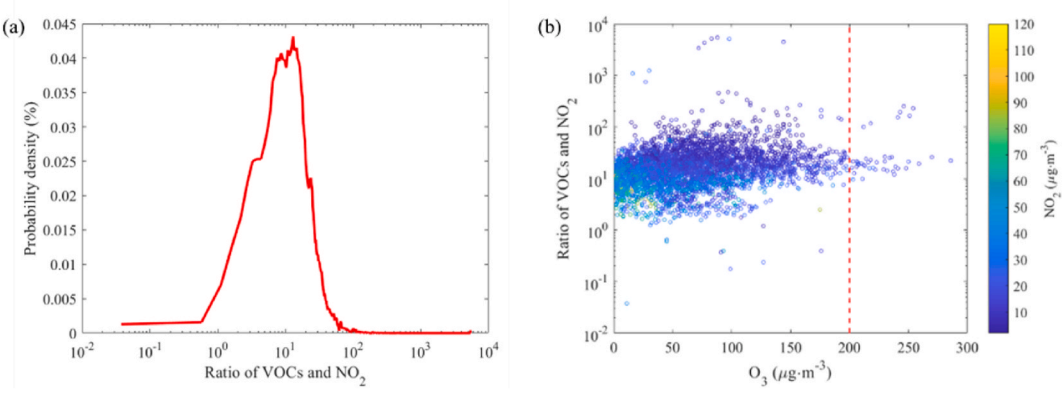

Fig. 5. The distribution of the ratio of VOCs and NO_2 by (a) the probability distribution and (b) the scatter distribution related to O_3 and NO_2 concentration.

centered around 13.0 and averagely of 28.3, indicating the local atmospheric condition most likely belonged to transition zone [41,53,56], together with some extremely high VOCs conditions.

As to the relation among the ratio, NO_2 and O_3, as shown in Fig. 5(b), when the concentration of NO_2 reached a sufficiently low level under about 20 μg m^{-3}, as shown in Fig. S4, the ratios exhibited a higher trend compared to conditions with higher level of NO_2 concentration. The ratio exhibited a clear decreasing trend with increasing NO_2 concentration. Moreover, severer O_3 pollution, exceeding 200 μg m^{-3} for instance, were often observed within two distinct ratio ranges of 9.5–26.3 and 99.8–251.6.

3.4. O_3 response to precursors

Considering the complex interaction between O_3 and precursors, as well as the different meteorological affection. The individual affection influence of precursor on O_3 concentration was simulated by the optimized RF model controlling other factors under a fixed atmospheric condition.

In order to elucidate the regulatory mechanisms behind elevated O_3 concentrations during daytime and enhance the accuracy of prediction simulations, investigations into O_3 formation mechanisms were conducted specifically at 15:00, which represents the daily average peak time according to the analysis on the distribution of daily O_3 concentration. Therefore, the concentrations of O_3 were simulated at different levels of NO_2 and VOCs with the optimized RF model, controlling consistent mild atmospheric conditions at average levels of meteorological elements and other pollutants concentration, that is, 2 μg m^{-3}, 0.5 mg m^{-3}, 13 μg m^{-3} and 20 μg m^{-3} for the concentration of SO_2, CO, $PM_{2.5}$ and PM_{10}, at T of 26 °C, P of 1007 Pa, RH of 50 %, WD of 225° and WS of 0.7 at time of 15, as shown in Fig. 6(a). The concentrations of O_3 were generally at a moderate degree under average atmospheric conditions and exhibited relatively stability at a certain NO_2 concentration while showing slight fluctuations with VOCs concentrations. The fluctuations caused by the variation in VOCs were higher compared to those caused by changes in NO_2, thereby elucidating the observed correlation between VOCs and O_3 at low NO_2 concentration levels. However, when NO_2 concentration was higher, the O_3 concentration decreased despite the change in VOCs concentration, resulting the weak correlation between VOCs and O_3. Interestingly, there were another stability O_3 concentration with the NO_2 concentration between 18 μg m^{-3} and 27 μg m^{-3}. When NO_2 concentration was higher than 27 μg m^{-3}, significant decrease was observed, exhibiting the strong affection of titration by NO_2. Furthermore, the whole range of O_3 was investigated by contour curves, different from the comprehensive expression of the EKMA curves, the contour curves exhibited the O_3 response to the variation of VOCs and NO_2 under a certain atmospheric condition. Under mild atmospheric condition, as shown in

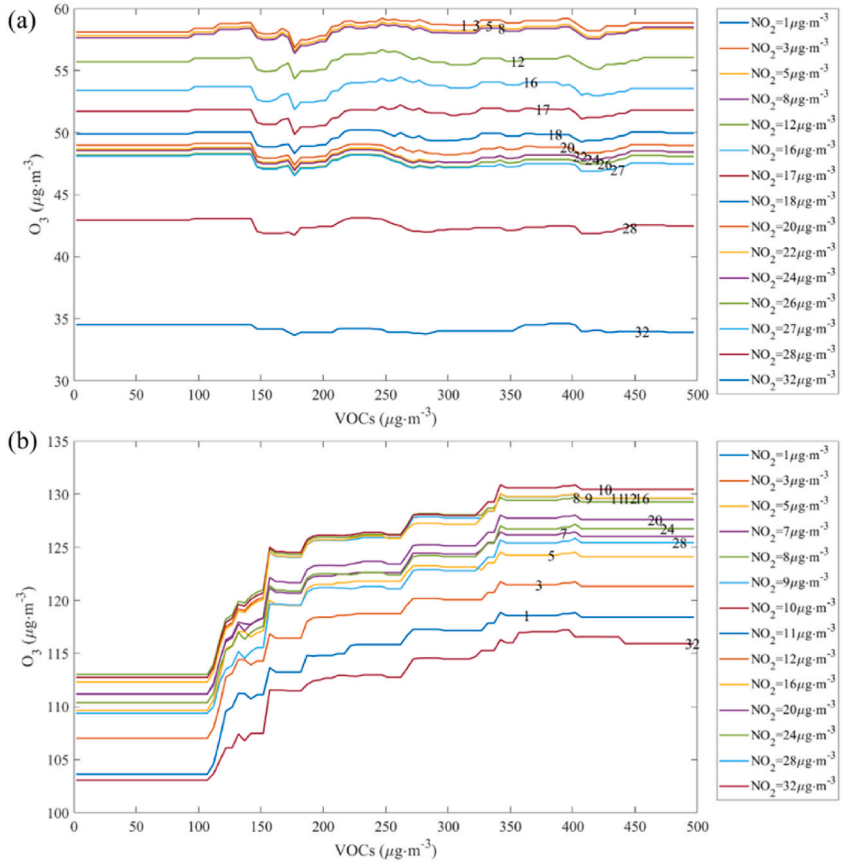

Fig. 6. O_3 simulation at different levels of NO_2 and VOCs under (a) mild atmospheric condition and (b) high reaction atmospheric conditions.

Fig. S5(a), the concentration contour was almost parallel to the axe of VOCs, indicating the weak influence on O_3 formation of VOCs. As to NO_2, a negative correlation to O_3 concentration was observed, and the O_3 concentration remained relatively low at 20 μg m^{-3} when NO_2 concentration exceeded 60 μg m^{-3}.

Then, when controlling the atmospheric under high reaction atmospheric conditions of relatively low RH at 50 % and high T at 35 °C, the concentrations of O_3 were simulated at different levels of NO_2 and VOCs with the optimized RF model. The O_3 concentration exhibited stronger fluctuation with both the variation of VOCs and NO_2 concentrations, as shown in Fig. 6(b). The O_3 concentration revealed an obvious elevation when VOCs concentration exceeding 110 μg m^{-3} under each level of NO_2 concentration. When VOCs concentration continually increase to 350 μg m^{-3} and higher, the O_3 concentration elevated slightly, indicating the oversaturation on VOCs concentration. Different from the monotone increasing affection of NO_2 concentration under mild atmospheric conditions, the O_3 concentration increased and then decreased in response to the increasing NO_2 concentration, displaying a characteristic inflection point at 10 μg m^{-3} under high reaction atmospheric conditions. Indicating the O_3 formation and titration affection dominates the reactions under low and high level of NO_2 concentration, respectively.

In addition, as shown in Fig. S5(b), the contour curves revealed more complex. When VOCs concentration was low, O_3 concentration was controlled by NO_2 due to the unsaturated VOCs, thus the O_3 concentration was hardly affected by VOCs. With the increasing in VOCs concentration, higher O_3 concentration was observed under a certain level of NO_2 concentration. As to NO_2, a significant transfer in the affection on O_3 concentration was observed at NO_2 concentration at 10 μg m^{-3}. In the view of chemical reaction process of the cycle among O_3 and NO*x* [57], under high reaction atmospheric conditions, more reactive radicals produced at higher VOCs concentration and continuing NO*x* cycle at lower NO_2 concentration, resulting in the acceleration in the direction of producing more O_3. Other study also indicate a less impact of VOCs concentration on O_3 compared to NO*x* concentrations, as well as different intensity of changes was observed at different NO*x* concentrations [35].

Furthermore, the atmospheric oxidant ($Ox = O_3 + NO_2$) was investigated under both the mild and high reaction atmospheric conditions, as shown in Fig. 7. The oxidant exhibited consistent response to the increasing in VOCs concentration of slight fluctuations and some elevation under the mild and high reaction atmospheric conditions, respectively, as shown in Fig. 7(a)and(b). However, the atmospheric oxidant acted different from O_3 concentrations with the variation of NO_2. The average concentrations of oxidant were calculated in the whole range of VOCs concentration, two peaks were observed at the NO_2 concentration of 16 μg m^{-3} and 27 μg m^{-3}. According to the photochemical reaction cycle of NO*x* ($NO_2 + O_2 \xleftrightarrow{h\nu} O_3 + NO$), the oxidant should be directly controlled by the emission of NO*x*, however, the oxidant levels were significantly higher under high reaction atmospheric conditions compared to mild conditions, where only RH and T varied, as shown in Fig. 7(c). Therefore, it is inferred that other oxidizing components existed, and the oxidizing power can be enhanced under high reaction atmospheric conditions. The affection on oxidant enhance can also be verified by the distribution of oxidant with variation of RH and T applying the monitoring data, as shown in Fig. S6. The oxidizing elevation increased 54 μg m^{-3} to 77 μg m^{-3} with the increasing in NO_2 concentration, owning an average elevation of 68 μg m^{-3} from mild to

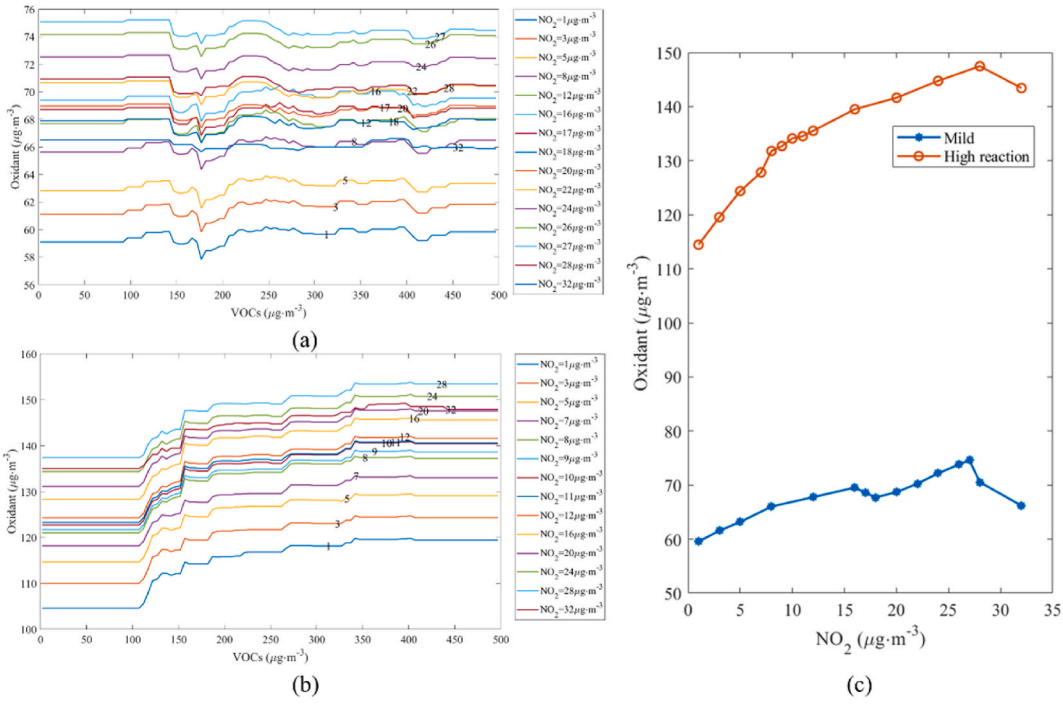

Fig. 7. Oxidant concentrations at different levels of NO_2 and VOCs of (a) mild atmospheric condition; (b) high atmospheric condition; (c) Oxidant concentrations under mild and high reaction atmospheric conditions.

high reaction atmospheric conditions.

4. Conclusion

This study conducted a comprehensive 1-year analysis applying the monitoring data from a standard continuous air quality monitoring station in Deqing county. The O_3 concentration peaked at 3 p.m., extremely high O_3 concentration were primarily observed when T exceeded 30 °C, and RH between 30 and 60 %. Similar high O_3 concentration conditions were reported in other systems [44]. Then, an optimized RF model was developed with exceptional performance in comparison to other O_3 prediction studies conducted in Tianjin and Zhejiang [35,44]. The importance analysis on O_3 prediction showed NO_2, RH and T were the top 3 important factors. Compared to the *Pearson* correlations results that the same top 3 highest correlations with O_3 concentration, but sorted differently of −0.55, 0.44 and −0.42 for RH, T and NO_2. Indicating O_3 concentration have better linearly relationship to RH and T, while stronger nonlinearly relationship to NO_2. Besides, VOCs with weak importance also revealed almost no correlation to both other factors and O_3 concentration. Another study carried out in Hangzhou also observed relatively low importance of VOCs concentration, as well as ozone formation potential and propene equivalent concentration [58].

The superiority and the efficacy of ML approaches in capturing the nonlinearity response of ozone to influential pollutants and meteorological factors have been demonstrated. By constraining the variable of time at 15:00 to figure out the formation mechanism under daily peak conditions of O_3 concentration, and setting the meteorological parameters under relatively stable conditions to weaken the influence from regional transport and diffusion, the response regulations were then examined using RF prediction under different precursor conditions. Under mild atmospheric conditions, at low NO_2 concentration levels, the fluctuations caused by the variation in VOCs were higher compared to those caused by changes in NO_2, thereby elucidating the observed correlation between VOCs and O_3. When NO_2 concentration exceeded 27 μg m^{-3}, significant decrease of O_3 concentration was observed, exhibiting the strong affection of titration by NO_2. Under controlled and consistent high reaction atmospheric conditions, the O_3 concentration revealed an obvious elevation when VOCs concentration exceeded 110 μg m^{-3}, and subsequently remained at relatively high level beyond 350 μg m^{-3}. The O_3 concentration displayed a characteristic inflection point at NO_2 concentration of 10 μg m^{-3}, indicating the O_3 formation and titration affection dominates the reactions under low and high level of NO_2 concentration, respectively. More reactive radicals produced at higher VOCs concentration and continuing NO*x* cycle at lower NO_2 concentration, resulting in the acceleration in the direction of producing more O_3. In addition, the oxidant levels were significantly higher under high reaction atmospheric conditions compared to mild conditions, suggesting the presence of other oxidizing components and an enhanced oxidizing power. Besides, the oxidizing elevation exhibited an average elevation of 68 μg m^{-3} from mild to high reaction atmospheric conditions. In conclusion, the local atmospheric conditions mostly belonged to NO*x*-sensitive and transition zone; the significant different O_3 response to variation of VOCs and NO*x* concentration between mild and high reaction atmospheric conditions, as well as the existing of oxidant elevation should be considered in local air quality control.

Moreover, given the escalating volume of data on pollutants and meteorological elements monitoring, efficient data analysis assumes increasing significance in uncovering profound patterns. The ML techniques applied in this study presents significant advantages in the realm of monitoring data visualization and the exploration of interrelationships during O_3 formation process. The formation of daily O_3 concentration peak varies with atmospheric conditions, but thanks to the comprehensive atmospheric monitoring network, and the utilization of only basic hourly monitored variables, this technique can be effectively implemented across different scales. Then, the findings can contribute to supplementing and enhancing the understanding of the local O_3 formation mechanism in a complex environment, as well as supporting an intuitional, rapid, and precise understanding on O_3 response for pollutants emission control.

Data availability statement

The data that has been used is confidential. Supplementary data to this article can be found online at https://doi.org/.

CRediT authorship contribution statement

Yan Huang: Writing – original draft, Validation, Resources, Methodology, Funding acquisition. **Qingqing Wang:** Validation, Investigation. **Xiaojie Ou:** Visualization, Validation, Data curation. **Dongping Sheng:** Investigation, Formal analysis. **Shengdong Yao:** Data curation. **Chengzhi Wu:** Writing – review & editing, Supervision, Methodology. **Qiaoli Wang:** Writing – review & editing, Writing – original draft, Supervision, Methodology, Funding acquisition, Conceptualization.

Declaration of competing interest

The authors declare that they have no known competing financial interests or personal relationships that could have appeared to influence the work reported in this paper.

Acknowledgments

This work was supported and funded by the National Key Research and Development Program of China (No. 2022YFC3703500), and the Public Welfare Application Research Project of Huzhou (No. 2022GZ61).

Appendix A. Supplementary data

Supplementary data to this article can be found online at https://doi.org/10.1016/j.heliyon.2024.e36303.

References

[1] X. Shi, Y. Zheng, Y. Lei, W. Xue, G. Yan, X. Liu, B. Cai, D. Tong, J. Wang, Air quality benefits of achieving carbon neutrality in China, Sci. Total Environ. 795 (2021) 148784, https://doi.org/10.1016/j.scitotenv.2021.148784.

[2] J. Mei, Y. Shen, Q. Wang, Y. Shen, W. Li, J. Zhao, J. Chen, S. Zhang, Roles of oxygen species in low-temperature catalytic o-xylene oxidation on MOF-derived bouquetlike CeO(2), ACS Appl. Mater. Interfaces 14 (31) (2022) 35694–35703, https://doi.org/10.1021/acsami.2c08418.

[3] Y. Lu, J. Hu, X. Yin, S. Qiao, S. Zhang, J. Ye, J. Chen, K. Feng, J. Zhao, Roles of biofilm structure and functional genes in overcoming limited dimethyl sulfide degradation and energy recovery, Acs Es&T Engineering (2024), https://doi.org/10.1021/acsestengg.3c00480.

[4] N. Cheng, D. Jing, C. Zhang, Z. Chen, W. Li, S. Li, Q. Wang, Process-based VOCs source profiles and contributions to ozone formation and carcinogenic risk in a typical chemical synthesis pharmaceutical industry in China, Sci. Total Environ. 752 (2021) 141899, https://doi.org/10.1016/j.scitotenv.2020.141899.

[5] X. Tan, L. Han, X. Zhang, W. Zhou, W. Li, Y. Qian, A review of current air quality indexes and improvements under the multi-contaminant air pollution exposure, J. Environ. Manag. 279 (2021) 111681, https://doi.org/10.1016/j.jenvman.2020.111681.

[6] Y. Wang, Y. Yuan, Q. Wang, C. Liu, Q. Zhi, J. Cao, Changes in air quality related to the control of coronavirus in China: implications for traffic and industrial emissions, Sci. Total Environ. 731 (2020) 139133, https://doi.org/10.1016/j.scitotenv.2020.139133.

[7] T. Xue, Y. Zheng, G. Geng, Q. Xiao, X. Meng, M. Wang, X. Li, N. Wu, Q. Zhang, T. Zhu, Estimating spatiotemporal variation in ambient ozone exposure during 2013-2017 using a data-fusion model, Environ. Sci. Technol. 54 (23) (2020) 14877–14888, https://doi.org/10.1021/acs.est.0c03098.

[8] X. Lu, J.Y. Hong, L. Zhang, O.R. Cooper, M.G. Schultz, X.B. Xu, T. Wang, M. Gao, Y.H. Zhao, Y.H. Zhang, Severe surface ozone pollution in China: a global perspective, Environ. Sci. Technol. Lett. 5 (8) (2018) 487–494, https://doi.org/10.1021/acs.estlett.8b00366.

[9] C. Zhang, D. Jing, C. Wu, S. Li, N. Cheng, W. Li, G. Wang, B. Chen, Q. Wang, J. Hu, Integrating chemical mass balance and the community multiscale air quality models for source identification and apportionment of PM2.5, Process Saf. Environ. Protect. 149 (2021) 665–675, https://doi.org/10.1016/j.psep.2021.03.033.

[10] D. Jing, N. Cheng, C. Zhang, Z. Chen, X. Cai, S. Li, J. Zhao, Q. Wang, W. Li, A novel approach for VOC source apportionment combining characteristic factor and pattern recognition technology in a Chinese industrial area, J. Environ. Sci. 121 (2022) 25–37, https://doi.org/10.1016/j.jes.2021.08.056.

[11] S. Wang, C. Zhou, Z. Wang, K. Feng, K. Hubacek, The characteristics and drivers of fine particulate matter (PM2.5) distribution in China, J. Clean. Prod. 142 (2017) 1800–1809, https://doi.org/10.1016/j.jclepro.2016.11.104.

[12] W. Li, L. Shao, W. Wang, H. Li, X. Wang, Y. Li, W. Li, T. Jones, D. Zhang, Air quality improvement in response to intensified control strategies in Beijing during 2013–2019, Sci. Total Environ. 744 (2020) 140776, https://doi.org/10.1016/j.scitotenv.2020.140776.

[13] Q. Wang, S. Li, M. Dong, W. Li, X. Gao, R. Ye, D. Zhang, VOCs emission characteristics and priority control analysis based on VOCs emission inventories and ozone formation potentials in Zhoushan, Atmos. Environ. 182 (2018) 234–241, https://doi.org/10.1016/j.atmosenv.2018.03.034.

[14] H. Qu, Y. Wang, R. Zhang, X. Liu, L.G. Huey, S. Sjostedt, L. Zeng, K. Lu, Y. Wu, M. Shao, M. Hu, Z. Tan, H. Fuchs, S. Broch, A. Wahner, T. Zhu, Y. Zhang, Chemical production of oxygenated volatile organic Compounds strongly enhances boundary-layer oxidation chemistry and ozone production, Environ. Sci. Technol. 55 (20) (2021) 13718–13727, https://doi.org/10.1021/acs.est.1c04489.

[15] Z. Tan, K. Lu, H. Dong, M. Hu, X. Li, Y. Liu, S. Lu, M. Shao, R. Su, H. Wang, Y. Wu, A. Wahner, Y. Zhang, Explicit diagnosis of the local ozone production rate and the ozone-NOx-VOC sensitivities, Sci. Bull. 63 (16) (2018) 1067–1076, https://doi.org/10.1016/j.scib.2018.07.001.

[16] W. Wei, S. Cheng, G. Li, G. Wang, H. Wang, Characteristics of ozone and ozone precursors (VOCs and NOx) around a petroleum refinery in Beijing, China, J. Environ. Sci. 26 (2) (2014) 332–342, https://doi.org/10.1016/s1001-0742(13)60412-x.

[17] D. Jing, K. Yang, Z. Shi, X. Cai, S. Li, W. Li, Q. Wang, Novel approach for identifying VOC emission characteristics based on mobile monitoring platform data and deep learning: application of source apportionment in a chemical industrial park, Heliyon 10 (8) (2024) e29077, https://doi.org/10.1016/j.heliyon.2024.e29077.

[18] Q. Wang, D. Sheng, C. Wu, D. Jing, N. Cheng, X. Cai, S. Li, J. Zhao, W. Li, J. Chen, A supplementary assessment system of AQI-V for comprehensive management and control of air quality in chemical industrial parks, J. Environ. Sci. 130 (2023) 114–125, https://doi.org/10.1016/j.jes.2022.06.037.

[19] K. Yang, W. Kong, X. Zhong, X. Cai, W. Luo, W. Li, S. Li, Q. Wang, Collaborative optimization of pollution and carbon reduction through carbon flow tracking integrated with life cycle assessment for petrochemical production, Chem. Eng. J. 488 (2024) 151123, https://doi.org/10.1016/j.cej.2024.151123.

[20] Q. Wang, D. Sheng, C. Wu, J. Zhao, F. Li, S. Yao, X. Ou, W. Li, J. Chen, Exploring ozone formation rules and concentration response to the change of precursors based on artificial neural network simulation in a typical industrial park, Heliyon 9 (9) (2023) e20125, https://doi.org/10.1016/j.heliyon.2023.e20125.

[21] Y. Yang, X. Liu, J. Zheng, Q. Tan, M. Feng, Y. Qu, J. An, N. Cheng, Characteristics of one-year observation of VOCs, NOx, and O3 at an urban site in Wuhan, China, J. Environ. Sci. (China) 79 (2019) 297–310, https://doi.org/10.1016/j.jes.2018.12.002.

[22] X. Chen, Y. Liu, A. Lai, S. Han, Q. Fan, X. Wang, Z. Ling, F. Huang, S. Fan, Factors dominating 3-dimensional ozone distribution during high tropospheric ozone period, Environ. Pollut. 232 (2018) 55–64, https://doi.org/10.1016/j.envpol.2017.09.017.

[23] K. Song, R. Liu, Y. Wang, T. Liu, L. Wei, Y. Wu, J. Zheng, B. Wang, S.C. Liu, Observation-based analysis of ozone production sensitivity for two persistent ozone episodes in Guangdong, China, Atmos. Chem. Phys. 22 (12) (2022) 8403–8416, https://doi.org/10.5194/acp-22-8403-2022.

[24] J. Xing, S. Zheng, D. Ding, J.T. Kelly, S. Wang, S. Li, T. Qin, M. Ma, Z. Dong, C. Jang, Y. Zhu, H. Zheng, L. Ren, T.-Y. Liu, J. Hao, Deep learning for prediction of the air quality response to emission changes, Environ. Sci. Technol. 54 (14) (2020) 8589–8600, https://doi.org/10.1021/acs.est.0c02923.

[25] N. Cheng, D. Jing, Z. Gu, X. Cai, Z. Shi, S. Li, L. Chen, W. Li, Q. Wang, Observation-based ozone formation rules by gradient boosting decision trees model in typical chemical industrial parks, Atmosphere 15 (5) (2024) 600, https://doi.org/10.3390/atmos15050600.

[26] K. Shukla, N. Dadheech, P. Kumar, M. Khare, Regression-based flexible models for photochemical air pollutants in the national capital territory of megacity Delhi, Chemosphere 272 (2021) 129611, https://doi.org/10.1016/j.chemosphere.2021.129611.

[27] S. Araki, M. Shima, K. Yamamoto, Spatiotemporal land use random forest model for estimating metropolitan NO2 exposure in Japan, Sci. Total Environ. 634 (2018) 1269–1277, https://doi.org/10.1016/j.scitotenv.2018.03.324.

[28] M. Gao, L. Yin, J. Ning, Artificial neural network model for ozone concentration estimation and Monte Carlo analysis, Atmos. Environ. 184 (2018) 129–139, https://doi.org/10.1016/j.atmosenv.2018.03.027.

[29] A. Sayeed, Y. Choi, E. Eslami, Y. Lops, A. Roy, J. Jung, Using a deep convolutional neural network to predict 2017 ozone concentrations, 24 hours in advance, Neural Network. 121 (2020) 396–408, https://doi.org/10.1016/j.neunet.2019.09.033.

[30] A. Yafouz, A.N. Ahmed, N.a. Zaini, M. Sherif, A. Sefelnasr, A. El-Shafie, Hybrid deep learning model for ozone concentration prediction: comprehensive evaluation and comparison with various machine and deep learning algorithms, Engineering Applications of Computational Fluid Mechanics 15 (1) (2021) 902–933, https://doi.org/10.1080/19942060.2021.1926328.

[31] H. Liu, Y. Xu, C. Chen, Improved pollution forecasting hybrid algorithms based on the ensemble method, Appl. Math. Model. 73 (2019) 473–486, https://doi.org/10.1016/j.apm.2019.04.032.

[32] H. Liu, H. Wu, X. Lv, Z. Ren, M. Liu, Y. Li, H. Shi, An intelligent hybrid model for air pollutant concentrations forecasting: case of Beijing in China, Sustain. Cities Soc. 47 (2019) 101471, https://doi.org/10.1016/j.scs.2019.101471.

[33] R. Ma, J. Ban, Q. Wang, Y. Zhang, Y. Yang, M.Z. He, S. Li, W. Shi, T. Li, Random forest model based fine scale spatiotemporal O(3) trends in the Beijing-Tianjin-Hebei region in China, 2010 to 2017, Environ. Pollut. 276 (2021) 116635, https://doi.org/10.1016/j.envpol.2021.116635.

[34] X. Ren, Z. Mi, P.G. Georgopoulos, Comparison of Machine Learning and Land Use Regression for fine scale spatiotemporal estimation of ambient air pollution: modeling ozone concentrations across the contiguous United States, Environ. Int. 142 (2020) 105827, https://doi.org/10.1016/j.envint.2020.105827.
[35] H. Xu, H. Yu, B. Xu, Z. Wang, F. Wang, Y. Wei, W. Liang, J. Liu, D. Liang, Y. Feng, G. Shi, Machine learning coupled structure mining method visualizes the impact of multiple drivers on ambient ozone, Communications Earth & Environment 4 (1) (2023), https://doi.org/10.1038/s43247-023-00932-0.
[36] S. Wang, Y. Sun, H. Gu, X. Cao, Y. Shi, Y. He, A deep learning model integrating a wind direction-based dynamic graph network for ozone prediction, Sci. Total Environ. 946 (2024) 174229, https://doi.org/10.1016/j.scitotenv.2024.174229.
[37] D. Yu, Z. Tan, K. Lu, X. Ma, X. Li, S. Chen, B. Zhu, L. Lin, Y. Li, P. Qiu, X. Yang, Y. Liu, H. Wang, L. He, X. Huang, Y. Zhang, An explicit study of local ozone budget and NOx-VOCs sensitivity in Shenzhen China, Atmos. Environ. 224 (2020) 117304, https://doi.org/10.1016/j.atmosenv.2020.117304.
[38] W. Wei, Y. Li, Y. Ren, S. Cheng, L. Han, Sensitivity of summer ozone to precursor emission change over Beijing during 2010–2015: a WRF-Chem modeling study, Atmos. Environ. 218 (2019) 116984, https://doi.org/10.1016/j.atmosenv.2019.116984.
[39] L. Zhang, L. Wang, D. Ji, Z. Xia, P. Nan, J. Zhang, K. Li, B. Qi, R. Du, Y. Sun, Y. Wang, B. Hu, Explainable ensemble machine learning revealing the effect of meteorology and sources on ozone formation in megacity Hangzhou, China, Sci. Total Environ. 922 (2024) 171295, https://doi.org/10.1016/j.scitotenv.2024.171295.
[40] L. Breiman, Random forests, Mach. Learn. 45 (1) (2001) 5–32, https://doi.org/10.1023/A:1010933404324.
[41] X. Yang, L. Gao, S. Zhao, G. Pan, G. Fan, Z. Xia, X. Sun, H. Xu, Y. Chen, X. Jin, Volatile organic Compounds in the north China plain: characteristics, sources, and effects on ozone formation, Atmosphere 14 (2) (2023), https://doi.org/10.3390/atmos14020318.
[42] V. Balamurugan, V. Balamurugan, J. Chen, Importance of ozone precursors information in modelling urban surface ozone variability using machine learning algorithm, Sci. Rep. 12 (1) (2022) 5646, https://doi.org/10.1038/s41598-022-09619-6.
[43] R. Dang, H. Liao, Y. Fu, Quantifying the anthropogenic and meteorological influences on summertime surface ozone in China over 2012-2017, Sci. Total Environ. 754 (2021) 142394, https://doi.org/10.1016/j.scitotenv.2020.142394.
[44] Q. Wang, D. Sheng, C. Wu, X. Ou, S. Yao, J. Zhao, F. Li, W. Li, J. Chen, Investigation of spatiotemporal distribution and formation mechanisms of ozone pollution in eastern Chinese cities applying convolutional neural network, J. Environ. Sci. 148 (2025) 126–138, https://doi.org/10.1016/j.jes.2023.09.001.
[45] K. Li, D.J. Jacob, H. Liao, J. Zhu, V. Shah, L. Shen, K.H. Bates, Q. Zhang, S. Zhai, A two-pollutant strategy for improving ozone and particulate air quality in China, Nat. Geosci. 12 (11) (2019) 906–910, https://doi.org/10.1038/s41561-019-0464-x.
[46] X. Lu, L. Zhang, Y. Chen, M. Zhou, B. Zheng, K. Li, Y. Liu, J. Lin, T.-M. Fu, Q. Zhang, Exploring 2016–2017 surface ozone pollution over China: source contributions and meteorological influences, Atmos. Chem. Phys. 19 (12) (2019) 8339–8361, https://doi.org/10.5194/acp-19-8339-2019.
[47] M.P. Vermeuel, G.A. Novak, H.D. Alwe, D.D. Hughes, R. Kaleel, A.F. Dickens, D. Kenski, A.C. Czarnetzki, E.A. Stone, C.O. Stanier, R.B. Pierce, D.B. Millet, T. H. Bertram, Sensitivity of ozone production to NOx and VOC along the lake Michigan coastline, J. Geophys. Res. Atmos. 124 (20) (2019) 10989–11006, https://doi.org/10.1029/2019jd030842.
[48] P. Wang, Y. Chen, J. Hu, H. Zhang, Q. Ying, Attribution of tropospheric ozone to NO (x) and VOC emissions: considering ozone formation in the transition regime, Environ. Sci. Technol. 53 (3) (2019) 1404–1412, https://doi.org/10.1021/acs.est.8b05981.
[49] W. Wei, X. Wang, X. Wang, R. Li, C. Zhou, S. Cheng, Attenuated sensitivity of ozone to precursors in Beijing-Tianjin-Hebei region with the continuous NO(x) reduction within 2014-2018, Sci. Total Environ. 813 (2022) 152589, https://doi.org/10.1016/j.scitotenv.2021.152589.
[50] A. Thielmann, A.S.H. Prévôt, F.C. Grüebler, J. Staehelin, Empirical ozone isopleths as a tool to identify ozone production regimes, Geophys. Res. Lett. 28 (12) (2001) 2369–2372, https://doi.org/10.1029/2000gl012787.
[51] S. Sillman, The use of NOy H2O2 and HNO3 as indicators for ozone-NOx-hydrocarbon sensitivity in urban locations, J. Geophys. Res. Atmos. 100 (14) (1995) 175–188.
[52] X.-x. Yang, L.-l. Tang, Y.-j. Zhang, Y.-f. Mu, M. Wang, W.-t. Chen, H.-c. Zhou, Y. Hua, R.-x. Jiang, Correlation analysis between characteristics of VOCs and ozone formation potential in summer in nanjing urban district, Huanjing Kexue 37 (2) (2016) 443–451.
[53] D. Shan, Z. Du, T. Zhang, X. Zhang, G. Cao, Z. Liu, Z. Yao, K. Tang, S. Liang, Variations, sources, and effects on ozone formation of VOCs during ozone episodes in 13 cities in China, Front. Environ. Sci. 10 (2023), https://doi.org/10.3389/fenvs.2022.1084592.
[54] S.L. Altshuler, T.D. Arcado, D.R. Lawson, Weekday vs. Weekend ambient ozone concentrations: discussion and hypotheses with focus on northern California, J. Air Waste Manag. Assoc. 45 (12) (2012) 967–972, https://doi.org/10.1080/10473289.1995.10467428.
[55] Y. Gao, F. Yan, M. Ma, A. Ding, H. Liao, S. Wang, X. Wang, B. Zhao, W. Cai, H. Su, X. Yao, H. Gao, Unveiling the dipole synergic effect of biogenic and anthropogenic emissions on ozone concentrations, Sci. Total Environ. 818 (2022), https://doi.org/10.1016/j.scitotenv.2021.151722.
[56] H. Qu, Y. Wang, R. Zhang, J. Li, Extending ozone-precursor relationships in China from peak concentration to peak time, J. Geophys. Res. Atmos. 125 (22) (2020), https://doi.org/10.1029/2020jd033670.
[57] T. Wang, L. Xue, P. Brimblecombe, Y.F. Lam, L. Li, L. Zhang, Ozone pollution in China: a review of concentrations, meteorological influences, chemical precursors, and effects, Sci. Total Environ. 575 (2017) 1582–1596, https://doi.org/10.1016/j.scitotenv.2016.10.081.
[58] R. Feng, H.J. Zheng, A.R. Zhang, C. Huang, H. Gao, Y.C. Ma, Unveiling tropospheric ozone by the traditional atmospheric model and machine learning, and their comparison: a case study in hangzhou, China, Environ. Pollut. 252 (Pt A) (2019) 366–378, https://doi.org/10.1016/j.envpol.2019.05.101.